Polymeric carbon nitride nanosheets/graphene hybrid phototransistors with high responsivity

*Sin Ki Lai, Chao Xie, Kar Seng Teng, Yanyong Li, Furui Tan, Feng Yan and Shu Ping Lau**

Sin Ki Lai, Dr. Chao Xie, Yanyong Li, Furui Tan, Prof. Feng Yan and Prof. Shu Ping Lau

Department of Applied Physics, The Hong Kong Polytechnic University, Hung Hom, Kowloon, Hong Kong SAR

E-mail: apsplau@polyu.edu.hk

Dr. Kar Seng Teng

College of Engineering, Swansea University, Bay Campus, Fabian Way, Crymlyn Burrows Swansea, SA1 8EN, United Kingdom

Keywords: g-C_3N_4, carbon nitride, graphene, photodetector, phototransistor

Abstract

Polymeric graphitic carbon nitride (g-C_3N_4) has emerged as a multi-purpose layered semiconductor. It can be processed into nanosheets by liquid phase exfoliation. In this work, g-C_3N_4 nanosheets were synthesized by a low-cost thermal condensation of melamine followed by ultrasonication. Phototransistors based on g-C_3N_4 nanosheets/graphene hybrid are reported for the first time. Synergistic effect is observed after combining the high mobility graphene and g-C_3N_4 that strongly absorbs in the entire UVA regime. Here, graphene acts as the carrier transport layer and g-C_3N_4 nanosheets form an active layer for exciton generation. The hybrid demonstrates efficient charge transfer from g-C_3N_4 nanosheets to graphene, which is verified by time-resolved photoluminescence, energy band analysis, transfer curve measurements, and is also consistent with reported computational studies. A responsivity of 4×10^3 A/W and a gain of the order 10^4 are observed under the illumination of ultraviolet light (wavelength is 370 nm). It is anticipated that the high performance g-C_3N_4 nanosheets/graphene hybrid phototransistors would find promising application in optoelectronics.

1. Introduction

Graphitic carbon nitride (g-C_3N_4) is a semiconductor with a layered structure that is analogous to graphite. It has an inter-layer distance of 0.32 nm, close to graphite (0.34 nm), and the layers are held by weak van der Waals force.[1] Unlike the gapless graphene, polymeric g-C_3N_4 has an inherent band gap of ~2.7 eV. Polymeric g-C_3N_4, simply denoted as g-C_3N_4, has disorders in the atomic structure with respect to the perfect heptazine-based g-C_3N_4 lattice **(**see supporting information **Figure S1)** due to the incomplete polymerization of the precursor.[1] Well-crystallized triazine-based g-C_3N_4 was reported by Algara-Siller et al. in 2014.[2] The synthesis requires a long heating time and a high pressure that remains up to 12 bar when the sealed ampoule was cooled to room temperature.[2] In comparison, the polymeric g-C_3N_4 can be synthesized by a low-cost and facile thermal condensation of nitrogen-rich precursors under atmospheric pressure.

In recent years, polymeric g-C_3N_4 has attracted enormous interest in hydrogen evolution reaction,[3,4] due to the suitable band structure of g-C_3N_4 with the water oxidation and reduction potentials situated in the bandgap. In addition, it can absorb ultraviolet (UV) light and has a marginal absorption (<450 nm) in the visible light regime.

On the other hand, the polymeric g-C_3N_4 process good optical property. It exhibits strong photoluminescence (PL) under UV excitation with a quantum yield (QY) of 7.92% measured in this work, and a QY of 19.6% reported in other work.[5] Light-emitting diodes and photovoltaic applications based on g-C_3N_4 have been reported,[6-8] the later revealed great potential of g-C_3N_4 for light harvesting applications. The strong PL implies that appreciable photocurrent should be generated if proper strategy is employed to separate the electron-hole pairs, which would be highly useful for photodetection and photovoltaics. ZnO nanostructure, being a popular choice for UV sensing material, has a bandgap of 3.37 eV,[9] which makes it less sensitive to the UVA spectral range from 3.1 to 3.3 eV, whereas this spectral range has

energy larger than the bandgap of g-C_3N_4. Additionally, g-C_3N_4 nanosheets only has marginal absorption in visible light, thus make it more suitable for near-ultraviolet detection than the small bandgap semiconductors.

One of the effective ways to separate electron-hole pairs is to construct hybrid materials. Owing to the energy offset of the valance and/or conduction band between the carefully designed hybrid components, a build-in potential can be found at their interfaces. Electrons and holes are driven in opposite direction under the potential, which can increase the dissociation efficiency of the bounded pairs. Hybrids of graphene and nanostructures are of particular interest since graphene can complement the low carrier mobility in nanostructures and is chemically stable with the nanostructures under light irradiation.[10] On the other hand, nanostructures absorb light more effectively than the one-atom thick graphene and can tune the absorption spectrum of the hybrid by selecting desirable nanostructures.[11-13]

It has also been reported that the g-C_3N_4 nanosheets showed a larger photoresponse than its bulk counterpart, which was attributed to an enhanced light absorption in the nanosheets.[5] However, g-C_3N_4 powders have shown to process a low conductivity of ~10^{-11} S/m,[14] which would significantly hinders the transport of photoexcited carriers in g-C_3N_4 and leads to large carrier loss via recombination.[7] With the motivation to harvest free carriers from g-C_3N_4 nanosheets, we were prompted to study the g-C_3N_4 nanosheets/graphene hybrid.

In this work, the g-C_3N_4 nanosheets/graphene hybrid phototransistor is reported. The hybrid devices show a high responsivity of the order 10^3 A/W, and a gain of 10^4 under UV illumination, which are comparable to the ZnO nanoparticles/graphene UV phototransistors with a responsivity of 10^4 A/W and a gain of 10^4,[9] and the perovskite/graphene UV to visible phototransistors with a responsivity of 10^2 A/W.[13] The enormous photoresponse of the hybrid is related to an efficient charge transfer from g-C_3N_4 nanosheets to graphene, which is evident from the time-resolved PL measurement, band diagram analysis and transfer curve measurements. With the facile preparation, in addition to the metal-free, earth abundant nature

of g-C_3N_4, it is anticipated that the g-C_3N_4 nanosheets/graphene hybrid would find useful applications in photodetection and photovoltaics.

2. Results and Discussion

2.1 Characterizations

The morphology of g-C_3N_4 nanosheets was investigated by transmission electron microscopy (TEM) as shown in **Figure 1 and Figure S2** (in the supporting information). As observed from the TEM images, the g-C_3N_4 nanosheets are irregular in shape with a lateral dimension ranging from 30 to 200 nm. Some sheets appear porous and crumpled. The thicknesses of the g-C_3N_4 nanosheets were further investigated by the atomic force microscope (AFM) as shown in **Figure 1c**. It can be seen that the thicknesses of the nanosheets are below 20 nm and the majority of them are 4 to 8 nm thick (see supporting information, **Figure S2d**). Liquid phase ultrasonication is therefore an effective and low-cost route for the exfoliation of g-C_3N_4. The distribution of g-C_3N_4 nanosheets dropped-casted on graphene was examined and is shown in **Figure S3**. In the AFM images, a few puckers originated from the foled graphene layer can be clearly observed. The graphene was smoothly transferred onto the SiO_2/Si substrate as seen from the similar height scale in Figure 1c and Figure S3a-b. The g-C_3N_4 nanosheets were also uniformly distributed on the graphene over large area as inferred from the scanning electron microscopy (SEM) image in Figure S3c.

The x-ray diffraction (XRD) of the g-C_3N_4 is shown in **Figure 2a**. The peak at 2θ = 27.5^o arises from the (002) planes of graphitic materials with conjugated aromatic structure. It corresponds to an interlayer distance of 0.324 nm, which is consistent with reported values.[3,4] The broad peak indicates possible stacking disorder that is known for stacking attracted by non-directional π - π interaction.[2] Another commonly observed, less distinctive (100) peak at 2θ = 12.9^o is assigned to the in-plane nitrogen repeating units with a distance of 0.686 nm.[4]

Fourier transform infrared spectroscopy (FTIR) of the g-C_3N_4 is shown in **Figure 2b**. The sharp absorption peak at 809 cm^{-1} is the characteristic out-of-plane vibration mode of the tri-*s*-triazine rings of g-C_3N_4.[15] The peaks at 1246 cm^{-1} and 1325 cm^{-1} are ascribed to the stretching vibration of C-N(-C)-C and C-NH-C bonds respectively.[5,15] The absorption band from 1400 to 1700 cm^{-1}, which consists of four peaks at 1410, 1463, 1571 and 1641 cm^{-1} are assigned to the stretching vibration modes of C=N and C-N bonds.[16]

Complementary to the FTIR study, X-ray photoelectron spectroscopy (XPS) was carried out to gain more insight on the chemical bonding of the C and N elements in the g-C_3N_4 nanosheets as shown in **Figure S4** in the supporting information. The full-scan spectrum in Figure S4(a) indicates the presence of mainly nitrogen and carbon, with a small amount of oxygen (2.2 at. %) in the g-C_3N_4 nanosheets. The C/N atomic ratio is 0.70, which is similar to the reported values on polymeric g-C_3N_4, ranging from 0.67-0.72.[8,15,17] A small oxygen content was commonly reported for polymeric g-C_3N_4,[5,16] which is ascribed to adsorbed water and oxygen on the nanosheets. The N-1s spectrum was deconvoluted into three peaks at 398.5, 400.2 and 404.6 eV. The dominant peak at 398.5 eV is originated from the sp^2-bonded N atoms (C=N-C) in the triazine ring. The peak at 400.2 eV is assigned to tertiary nitrogen in $N(-C)_3$ and H-$N(-C)_2$ bonding.[15,16,18] A much weaker peak at 404.6 eV can be related to charge localization in cyano- group.[19] The C-1s spectrum was fitted with two peaks at 284.6 and 288.0 eV. The major peak at 288.0 eV corresponds to sp^2 carbon in $N=C(-N)_2$. The weaker peak at 284.6 eV is assigned to adventitious carbon (C=C) in the graphitic domains.[15] The g-C_3N_4 nanosheets exhibit a blue PL under UV excitation as shown in **Figure 2c** and the inset of **Figure 2d**. The PL intensity grew larger when the excitation wavelength is increased from 325, 350 to 375 nm, which can be related to an increase in absorption from 325 to 375 nm in reference to the UV-visible spectrum in **Figure 2f**. The PL peak locates at ~440 nm. The PL quantum yield of g-C_3N_4 nanosheets was measured to be 7.92%. One of the key issues in photovoltaic, photocatalysis and photodetection is to extract the charge carriers

generated under irradiation. Formation of hybrid materials have shown to be an effective way to quench the PL by a charge transfer. [14,20,21] Several computational studies have already predicted significant charge transfer between graphene and g-C_3N_4 monolayer due to the creation of electron-hole puddles between the g-C_3N_4 and graphene interface as a consequence of the non-uniform electron distribution in g-C_3N_4 lattice.[22,23] **Figure 2d** shows the time-resolved PL of pristine g-C_3N_4 nanosheets and g-C_3N_4/graphene hybrid. The average decay lifetime of pristine g-C_3N_4 and the hybrid were calculated to be 4.34 and 3.90 ns respectively, where the parameters and calculation method are provided in **Table S1** in the supporting information. The PL decay lifetime of the g-C_3N_4/graphene hybrid is shorter than that of the pristine g-C_3N_4 nanosheets as a result of a rapid transfer of charges at a timescale shorter than the PL lifetime which would suppress the radiative recombination in the hybrid,[24] thus this indicates a charge transfer from g-C_3N_4 nanosheets to graphene.

The Raman spectrum of g-C_3N_4 nanosheets, graphene and their hybrid is shown in **Figure 2e**. The g-C_3N_4 shows a strong fluorescence background under the 488 nm probe laser. Graphene demonstrates a G peak at 1590 cm^{-1}, which originates from the in-plane vibrations of sp^2 carbon.[24] The 2D peak at 2700 cm^{-1} is related to the second order scattering at the Brillouin zone boundary of graphene.[26] An I_{2D}/I_G ratio larger than two indicates that it is monolayer graphene. No apparent difference was observed in the spectrum after drop-casting g-C_3N_4 nanosheets onto graphene, in particular the intensity of D peak at 1350 cm^{-1}, which is related to defects in graphene, remains low, indicates that the quality of graphene was not affected by the deposition of g-C_3N_4.

The UV-visible diffuse reflectance spectrum of g-C_3N_4 was measured, and was converted to absorption spectrum using the Kubelka-Munk function (F(R)), as shown in **Figure 2f**. The resultant F(R) values are proportional to the absorption coefficient. Absorption starts at ~440 nm, and peaks at 385 nm. It absorbs strongly throughout the UVA spectral range.The Tauc plot was further analyzed and is given in the inset of **Figure 2f**, where a direct band gap was

taken, and the optical band gap was determined to be 2.84 eV, which coincides with the PL emission peak at ~440 nm.

2.2 Device measurements

The schematic diagram of the device structure is shown in **Figure 3a**. Heavily-doped Si substrate serve as the back gate in field effect measurements. The detailed device fabrication procedure is provided in the experimental section. To eliminate doping from atmospheric oxygen and water vapors, measurements were conducted in a nitrogen atmosphere unless otherwise specified.

When illuminated with UV light, the transfer curve shifts towards negative gate voltage (V_G), as shown in **Figure 3b**. When light intensity increases, the number of photo-generated charge carriers in g-C_3N_4 increases, the transfer curves of graphene shift to more negative V_G. This is analogous to a progressive n-doping of graphene.[9] After revealing a charge transfer from g-C_3N_4 to graphene in the time-resolved PL, based on the shift direction of the transfer curves, we can further determine that electron is the type of carrier transferred to graphene. This is further supported by the energy band diagram as shown in **Figure 3c**. The Fermi level of graphene was reported to be at ~4.6 eV.[27] From the ultraviolet photoelectron spectroscopy (UPS) measurement of g-C_3N_4 nanosheets provided in **Figure S4d**, the valence band edge (VB) was determined to be at -7.3 eV. Using the optical band gap, the conduction band edge was determined to be at -4.46 eV. The Fermi level (E_F) of g-C_3N_4 is ~2.39 eV above VB.[28] A built-in electric field exists at the g-C_3N_4/graphene interface due to band bending resulted from the offset of energy levels. Under irradiation, the electric field promotes electron-hole pairs dissociation at the interface. Electrons are transferred to graphene under the drift of the internal field, while holes are trapped in g-C_3N_4 nanosheets. The holes in g-C_3N_4 induce a negative charge in graphene through capacitive coupling, which is effectively analogous to applying a positive gate voltage on graphene.[11] Due to the trapping of positive charges in g-

C_3N_4, electrons circulate multiple times in the high mobility graphene channel before recombination, giving rise to the photoresponse and a high gain in the devices, [11] where the gain would be further discussed below. This photogating effect elucidates the photosensing mechanism of the device.

Figure 3d shows that the photocurrent of the device can be controlled to a great extent by the gate voltage. The sign of photocurrent changes from negative to positive as the gate voltage sweeps through the Dirac point. Near the Dirac Point, the photocurrent is zero. The device is effectively turned 'off' by the gate voltage. The zero photocurrent is explained by the same density of conducting elelctrons and holes in the illuminated and dark device respectively, as depicted in the figure. The gate voltage has an additionally function to switch the sign of the photocurrent (or the resistance change), which, unlike the source-drain voltage, can only tune the magnitude of the photocurrent in the device. The variation of responsivity with the incident wavelength of light is shown in **Figure 4a**. It shows a trend similar to the absorption of the g-C_3N_4 nanosheets as expected. A high responsivity was found for wavelength shorter than ~410 nm, thus demostrates that the hybrid devices are especially suitable for UVA detection.

Figure 4b shows that the photocurrent (I_{Ph}) increases linearly with the source-drain bias (V_{DS}), where the applied V_G is 5 V. The transit time (τ_{tr}) of electrons in the graphene channel is related to V_{DS} by the relation $\tau_{tr} = L^2/\mu V_{DS}$, where μ is the carrier mobility, L is the channel length.[29] Under constant light intensity, increase in V_{DS} shortens the electron transit time, and leads to higher photocurrent and thus the responsivity. The responsivity (R) is given by $R = I_{Ph}/P$, where P is the incident light power. As shown in **Figure 5a**, the responsivity increases noticeably when light intensity decreases, which is commonly observed in photodetectors.[12,13,30] An increase in the concentration of photo-generated charge carriers creates an electric field that is opposite to the built-in electric field, which retards the charge separation. At the lowest light intensity investigated in this work, the responsivity reaches

4×10^3 AW^{-1}. Responsivity much larger than 1 AW^{-1} implies more than one charge carrier is detected from one photon striking the device. This parameter is quantitatively described by the gain (G), which can be related to R by the relation $R = I_{Ph}/P = \eta qG/h\nu$,[29] where ν is the light frequency, q is the electron charge, η is the external quantum efficiency. Considering that η should be less than 100%, the gain of the device is estimated to be at least of the order of 10^4.

Photodetectors should export different magnitudes of photocurrent or photovoltage under different light intensities, which is important for practical sensing applications. The photocurrent of the devices increases non-linearly yet monotonically with light intensity **(Figure 5b)** and can be described by the relation $I_{Ph} = W^{\theta}$, where $\theta = 0.39$ from the fitting result. The non-linearity could be related to an increase in carrier recombination at stronger light intensity, as discussed in earlier section. This increase in recombination at higher intensity can also be due to the presence of trap states in the material.[31] Defects in the g-C_3N_4 nanosheets could be an origin of these trap states,[32-33] which were generated during the thermal polymerization of the g-C_3N_4.[1,33] At higher light intensity, the traps are filled, the number of free carrier increases which results in a higher probability of recombination.[31,34-36]

The temporal photoresponse under on/off cycles is shown in **Figure 5c**, where the applied V_G is 8 V and V_{DS} is 0.5 V. The g-C_3N_4 nanosheets/graphene hybrid exhibits a large, positive photocurrent of about 15 μA upon illumination (light blue region), and recover back to the dark current level when light is off, this demonstrates the reproducibility of photoresponse in the hybrid devices. On the other hand, for the graphene-only control device, a small negative photocurrent, which is in contrast to the positive photocurrent in the hybrid device, can be observed under prolonged illumination at the same biasing condition. The result clearly demonstrates the important role of g-C_3N_4 nanosheets on the photoresponse of the hybrid. By utilizing the advantage of individual component, i.e. the strong UV absorption of g-C_3N_4 nanosheets and the high mobility of graphene, the hybrid structure exhibit synergistic effect

which outperforms their individual component. g-C_3N_4 nanosheets acts as the active layer for electron-hole pairs generation, and graphene acts as the carrier transport layer in the device. The highly efficient charge transfer from g-C_3N_4 nanosheets to graphene enables a strong photogating effect in graphene and results in the large photoresponse observed.

Photoresponse is also measured in the ambient condition, as shown in **Figure S5** in the supporting information. A negative photocurrent is observed, and no positive photocurrent can be obtained upon tuning the gate voltage between ±60V. This demonstrated that similar to other nanostructures,[9,35] the g-C_3N_4 nanosheets/graphene hybrid interact strongly with molecules in atmosphere due to their large surface-to-volume ratio. As seen from **Figure S5a**, the negative photoresponse is also reproducible, and has an enhanced negative photocurrent contributed by g-C_3N_4 nanosheets as compared to the graphene-only device as seen from **Figure S5b**. UV excitation invoke oxygen or hydroxyl groups related impurity scattering in graphene, which reduces the hole mobility in graphene.[36] The oxygen and hydroxyl groups are originated from the oxygen and water molecules adsorbed on graphene respectively. UV illumination promotes the desorption of negatively-charged oxygen molecules by capturing photogenerated holes, [9,35] which is more likely to occur at the surface of g-C_3N_4 nanosheets as it is exposed and is more photo-responsive. The loss of holes make g-C_3N_4 more negative and may act as additional scattering sites to the holes in graphene, which further decrease its mobility and results in the negative photocurrent. The situation is schematically depicted in **Figure S6** in the supporting information.

The response time of the device is analyzed in **Figure 5d**. The rise and decay response were fitted separately with the equation $I(t) = I_{dark} + A_1 exp(t/\tau_{r1}) + A_2 exp(t/\tau_{r2})$ and $I(t) = I_{dark} + A_3 exp(-t/\tau_{d1}) + A_4 exp(-t/\tau_{d2})$, where $\tau_{r1,2}$ and $\tau_{d1,2}$ are the rise and decay time constants respectively. It has a modest rise time constant of 0.74 s and a significantly slower recovery time, which is about ten times slower than the rise time. The values are given in the figure.

The longer decay time can be explained by the trapping of carriers in g-C_3N_4 nanosheets that leads to a slow relaxation of the photogating effect in graphene.

The stability of the hybrid phototransistors over time was further investigated. Photoresponse of the device that had been stored in the ambient air for more than 130 days are shown in **Figure S7**. A responsivity of an order 10^3 A/W and a reproducible photocurrent towards on/off cycles of light can still be obtained, thus the g-C_3N_4 nanosheets/graphene hybrid does not show obvious degradation over time and is highly stable for photodetectors application.

3. Conclusion

In conculsion, a large photocurrent and a high gain are demonstrated from the g-C_3N_4 nanosheets/graphene hybrid. This is enabled by a charge transfer from g-C_3N_4 nanosheets to graphene, which echos with reported computational studies. It is revealed in this work that the g-C_3N_4 naosheets/graphene hybrid is a high performance material for UVA detection. Development of the optoelectronic and photovoltaic applications of g-C_3N_4 is still in an early stage. With more efforts devoted to understanding the effect of morphology and defects of polymeric g-C_3N_4 on the photoresponse, and to synthesizing g-C_3N_4 nanosheets with a controllable morphology and defect density, further enhancement in the performance of the hybrid would be expected. Nonetheless, the hybrid, which is metal-free, comprised of only earth-abundant elements, and can be prepared with facile means, has shown to be an attractive alternative to popular materials reported for UV sensing such as ZnO and TiO_2.

4. Experimental section

Preparation of polymeric g-C_3N_4: 5 g of melamine (99%, Aladdin Reagents) was transferred to an alumina crucible covered with a lid. It was heated at 550 ^oC for 4 hrs at a ramp rate of 2 ^oC/min in static air, and cooled to room temperature at 2 ^oC/min. Melamine condensed into polymeric g-C_3N_4 in this process. A yellowish solid was obtained, and was grinded to

powders. Thermal oxidation etching was further carried out to etch the g-C_3N_4 into thinner sheets.[37] 400 mg of the powders was heated in an open crucible at 500 ^oC for 2 hrs at a ramp and cooling rate of 2 ^oC/min. The obtained g-C_3N_4 powders were dispersed in IPA at a concentration of 1 mg/ml, and was ultrasonicated for 12 hrs and then centrifuged at 3000 rpm for 10 min. The supernatant was collected and the g-C_3N_4 nanosheets were used for device fabrication.

Fabrication and measurements of devices: Graphene was grown by chemical vapor deposition on copper foil using methane as a precursor and H_2/Ar mixture as carrier gas in a tube furnace. PMMA was used as a protective layer during graphene transfer. Copper foil was dissolved in ammonium persulfate (0.1 M) solution overnight. The graphene/PMMA was transferred to DI water bath for 3 times before finally transferred to 300 nm SiO_2/Si substrate. It was dried in ambient condition overnight and then heated at 110 ^oC for 15 min to enhance the adhesion of graphene to the substrate. PMMA was dissolved in 60 ^oC acetone bath for at least 4 hrs. Interdigitated electrodes were fabricated on graphene using standard photolithography process. The electrodes consisted of 21 fingers, each with a width of 25 μm, a separation of 15 μm and a length of 1150 μm. Au (~100 nm) was deposited by thermal evaporation and the photoresist was lifted-off in acetone. 150 μl of g-C_3N_4 solution was dropped-casted onto the electrodes and the solvent was evaporated at 65 ^oC. The device was then transferred to a nitrogen-filled glove box and was heated at 150 ^oC for 2 hrs to remove adsorbates before measurements. Electrical measurements were carried out with a semiconductor parameter analyzer (Agilent 4156C) and the light source was a 370 nm LED. In wavelength-dependent responsivity measurement, the light sources were five LEDs with peak wavelength at 410, 550, 660, 895 and 940 nm. Optical power was measured with a calibrated power meter.

Supporting Information

Supporting Information is available from the Wiley Online Library or from the author.

Acknowledgements

The authors acknowledge Dr. Wei Lu for the TEM measurements. This work was financially supported by the Research Grants Council of Hong Kong (Project Nos. PolyU 5006/12P and PolyU 153012/14P), and PolyU grant (1-ZE14).

Received: ((will be filled in by the editorial staff))
Revised: ((will be filled in by the editorial staff))
Published online: ((will be filled in by the editorial staff))

[1] X. Wang, S. Blechert and M. Antonietti, *ACS Catal.* **2012**, *2*, 1596.
[2] G. Algara-Siller, N. Severin, S. Y. Chong, T. Björkman, R. G. Palgrave, A. Laybourn, M. Antonietti, Y. Z. Khimyak, A. V. Krasheninnikov, J. P. Rabe, U. Kaiser, A. I. Cooper, A. Thomas and M. J. Bojdys, *Angew. Chem. Int. Ed.* **2014**, *53*, 7450.
[3] X. Wang, K. Maeda, A. Thomas, K. Takanabe, G. Xin, J. M. Carlsson, K. Domen and M. Antonietti, *Nature Mater.* **2009**, *8*, 76.
[4] J. Liu, Y. Liu, N. Liu, Y. Han, X. Zhang, H. Huang, Y. Lifshitz, S. T. Lee, J. Zhong and Z. Kang, *Science* **2015**, *347*, 970.
[5] X. Zhang, X. Xie, H. Wang, J. Zhang, B. Pan and Y. Xie, *J. Am. Chem. Soc.* **2013**, *135*, 18.
[6] J. Xu, M. Shalom, F. Piersimoni, M. Antonietti, D. Neher and T. J. K. Brenner, *Adv. Optical Mater.* **2015**, *3*, 913.
[7] J. Xu, T. J. K. Brenner, L. Chabanne, D. Neher, M. Antonietti and M. Shalom, *J. Am. Chem. Soc.* **2014**, *136*, 13486.
[8] Y. Zhang, T. Mori, L. Niu and J. Ye, *Energy Environ. Sci.* **2011**, *4*, 4517.
[9] W. Guo, S. Xu, Z. Wu, N. Wang, M. M. T. Loy and S. Du, *Small* **2013**, *9*, 3031.
[10] K. T. Nguyen, D. Li, P. Borah, X. Ma, Z. Liu, L. Zhu, G. Grüner, Q. Xiong and Y. Zhao, *ACS Appl. Mater. Interfaces* **2013**, *5*, 8105.
[11] G. Konstantatos, M. Badioli, L. Gaudreau, J. Osmond, M. Bernechea, F. Pelayo Garcia de Arquer, F. Gatti and F. H. L. Koppens, *Nature Nanotech.* **2012**, *7*, 363.
[12] Z. Sun, Z. Liu, J. Li, G. A. Tai, S.P. Lau and F. Yan, *Adv. Mater.* **2012**, *24*, 5878.
[13] Y. Lee, J. Kwon, E. Hwang, C. H. Ra, W. J. Yoo, J. H. Ahn, J. H. Park and J. H. Cho, *Adv. Mater.* **2015**, *27*, 41.
[14] Y. Zhang, T. Mori, J. Ye and M. Antonietti, *J. Am. Chem. Soc.* **2010**, *132*, 6294.
[15] D. Gao, Q. Xu, J. Zhang, Z. Yang, M. Si, Z. Yan and D. Xue, *Nanoscale* **2014**, *6*, 2577.
[16] H. Xu, J. Yan, X. She, L. Xu, J. Xia, Y. Xu, Y. Song, L. Huang and H. Li, *Nanoscale* **2014**, *6*, 1406.
[17] W. Ho, Z. Zhang, W. Lin, S. Huang, X. Zhang, X. Wang and Y. Huang, *ACS Appl. Mater. Interfaces* **2015**, *7*, 5497.
[18] Q. Xiang, J. Yu and M. Jaroniec, *J. Phys. Chem. C* **2011**, *115*, 7335.
[19] S. Yang, Y. Gong, J. Zhang, L. Zhan, L. Ma, Z. Fang, R. Vajtai, X. Wang and P. M. Ajayan, *Adv. Mater.* **2013**, *25*, 2452.
[20] R. Saran, M. N. Nordin and R. J. Curry, *Adv. Funct. Mater.* **2013**, *23*, 4149.
[21] L. Peng, L. Hu and X. Fang, *Adv. Funct. Mater.* **2014**, *24*, 2591.

[22] A. Du, S. Sanvito, Z. Li, D. Wang, Y. Jiao, T. Liao, Q. Sun, Y. H. Ng, Z. Zhu, R. Amal and S. C. Smith, *J. Am. Chem. Soc.* **2012**, *134*, 4393.
[23] X. Li, Y. Dai, Y. Ma, S. Han and B. Huang, *Phys. Chem. Chem. Phys.* **2014**, *16*, 4230.
[24] R. Wang, L. Gu, J. Zhou, X. Liu, F. Teng, C. Li, Y. Shen and Y. Yuan, *Adv. Mater. Interfaces*, **2015**, *2*, 150037.
[25] S. K. Lai, L. Tang, Y. Y. Hui, C. M. Luk and S. P. Lau, *J. Mater. Chem. C* **2014**, *2*, 6971.
[26] Y. Y. Hui, G. Tai, Z. Sun, Z. Xu, N. Wang, F. Yan and S. P. Lau, *Nanoscale* **2012**, *4*, 3118.
[27] Y. J. Yu, Y. Zhao, S. Ryu, L. E. Brus, K. S. Kim and P. Kim, *Nano Lett.* **2009**, *9*, 3430.
[28] J. Chen, S. Shen, P. Guo, P. Wu and L. Guo, *J. Mater. Chem. A* **2014**, *2*, 4605.
[29] F. Liu and S. Kar, *ACS Nano* **2014**, *8*, 10270.
[30] S. K. Lai, C. M. Luk, L. Tang, K. S. Teng and S. P. Lau, *Nanoscale* **2015**, *7*, 5338.
[31] C. Soci, A. Zhang, B. iang, S. A. Dayeh, D. P. R. Aplin, J. Park, X. Y. Bao, Y. H. Lo and D. Wang, *Nano Lett.* **2007**, *7*, 1003.
[32] X. Li, G. Hartley, A. J. Ward, P. A. Young, A. F. Masters and T. Maschmeyer, *J. Phys. Chem. C* **2015**, *119*, 14938.
[33] P. Wu, J. Wang, J. Zhao, L. Guo and F. E. Osterloh, *J. Mater. Chem. A* **2014**, *2*, 20338.
[34] W. Zhang, J. K. Huang, C. H. Chen, Y. H. Chang, Y. J. Cheng and L. J. Li, *Adv. Mater.* **2013**, *25*, 3456.
[35] K. Zheng, F. Meng, L. Jiang, Q. Yan, H. H. Hng and X. Chen, *Small* **2013**, *9*, 2076.
[36] C. Biswas, F. Günes, D. D. Loc, S. C .Lim, M. S. Jeong, D. Pribat and Y. H. Lee, *Nano Lett.* **2011**, *11*, 4682.
[37] P. Niu, L. Zhang, G. Liu and H. M. Cheng, *Adv. Funct. Mater.* **2012**, *22*, 4763.

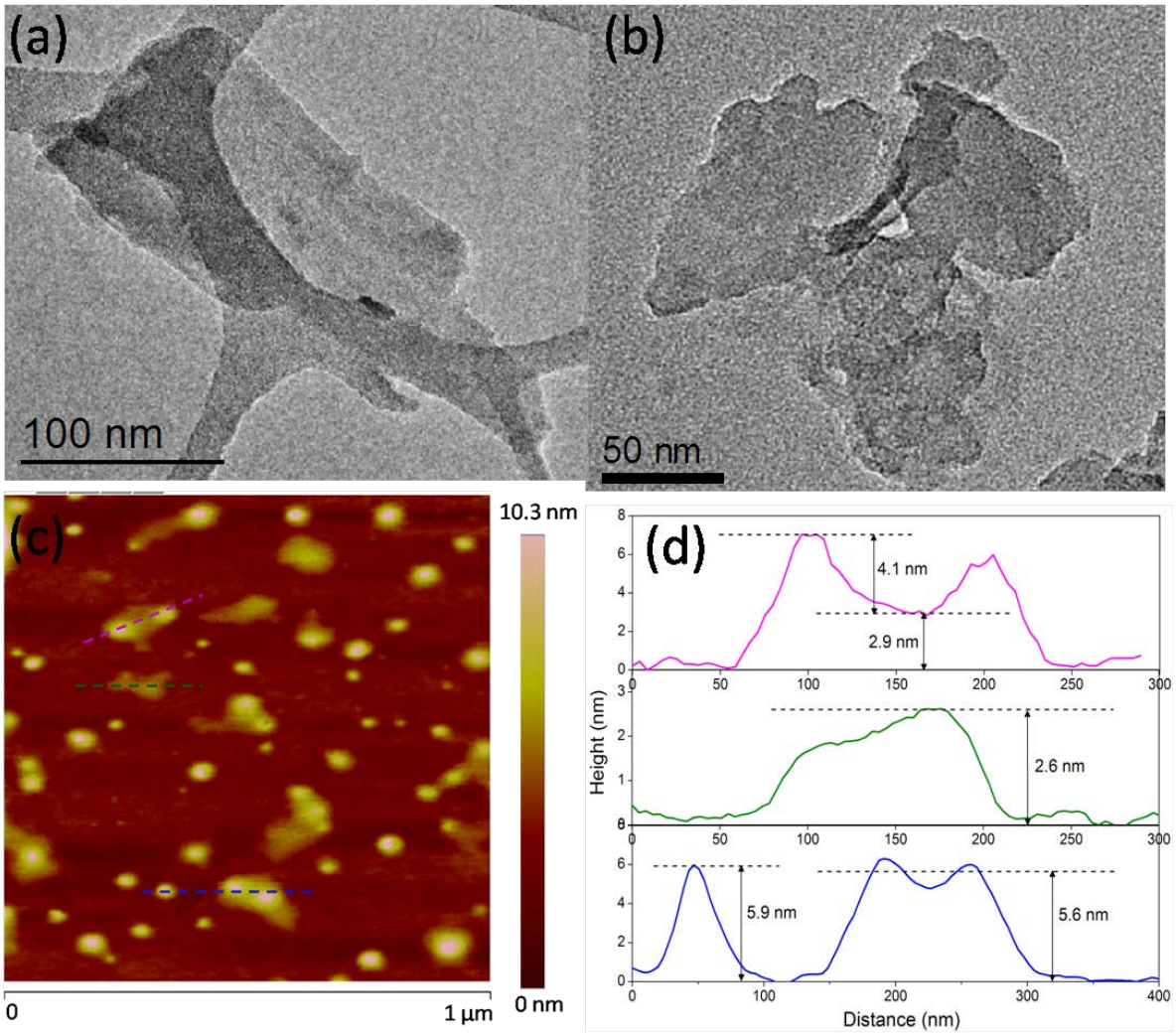

Figure 1. (a-b) TEM images of g-C_3N_4 nanosheets. Some sheets show a porous and crumpled morphology with a lateral dimension ranging from 30 to 200 nm. (c) AFM image of g-C_3N_4 nanosheets dispersed on SiO_2/Si substrate and (d) the corresponding height analysis showing the thicknesses of nanosheets are mostly below 10 nm.

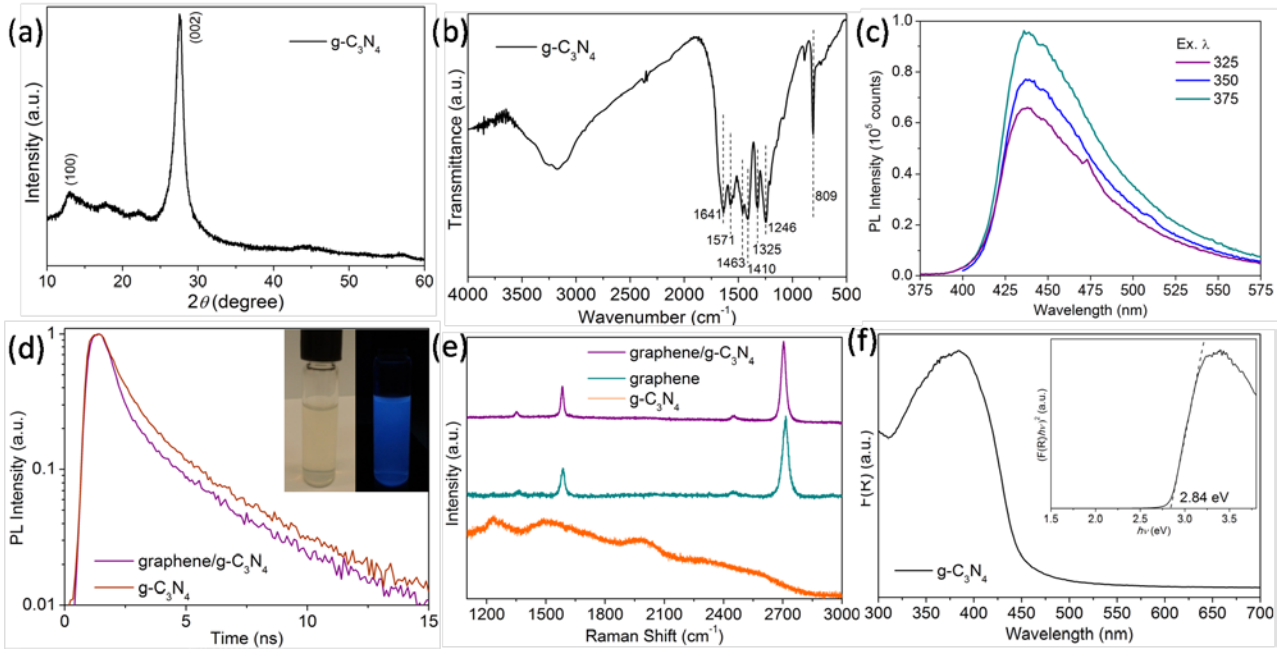

Figure 2. (a) XRD pattern of the g-C_3N_4 powders, the (002) peak corresponds to the interference from interlayer stacking. (b) FTIR spectrum of the g-C_3N_4 powders. The peak at 809 cm^{-1} is the characteristic peak of g-C_3N_4 arises from the tri-*s*-triazine ring vibration. (c) PL spectrum of the g-C_3N_4 nanosheets under UV excitation, with the PL peak situates at ~440 nm. (d) Time-resolved PL spectrum of pristine g-C_3N_4 nanosheets and the g-C_3N_4 nanosheets/graphene hybrid. Inset: Optical image of the dispersion of g-C_3N_4 nanosheets under normal lighting (left) and under 365 nm UV light (right). (e) Raman spectrum of g-C_3N_4, graphene and the hybrid. The excitation laser has a wavelength of 488 nm. (f) UV-visible absorption spectrum of the g-C_3N_4 converted from the diffuse reflectance spectrum. Inset: Tauc plot of g-C_3N_4 which gives an optical bandgap of 2.84 eV.

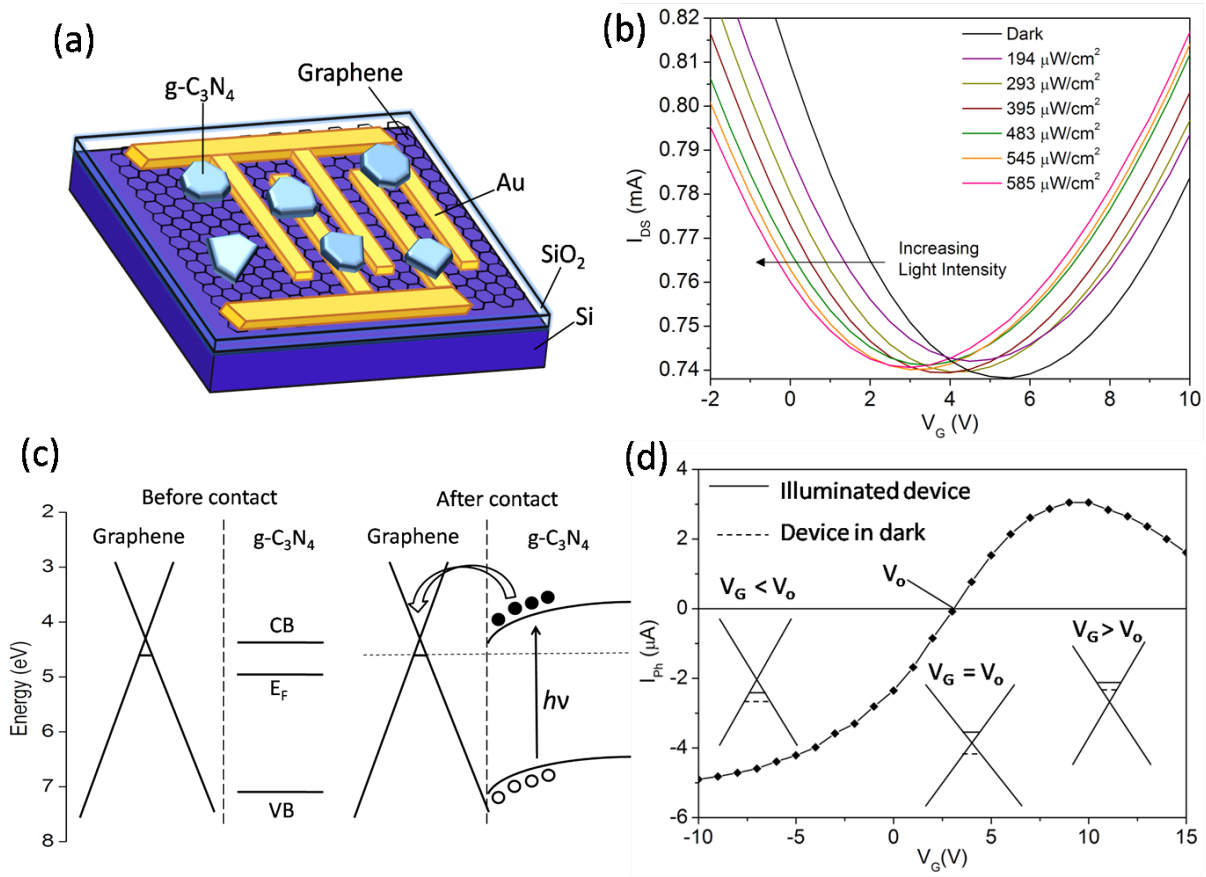

Figure 3. (a) Schematic diagram of the device structure. (b) Transfer curves of the device under different light intensities. The applied V_{DS} is 0.5 V and excitation wavelength is 370 nm. (c) Band diagram analysis of the g-C_3N_4 nanosheets/graphene hybrid. (d) Photocurrent as a function of the gate voltage. V_O denotes the gate voltage where photocurrent is zero.

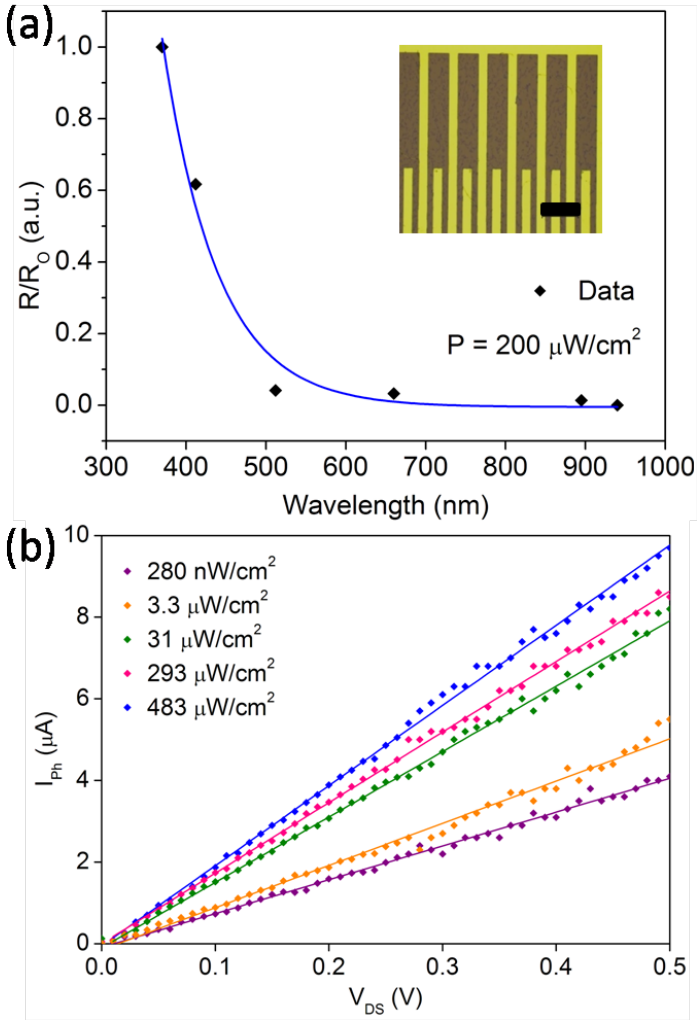

Figure 4. (a) Variation of responsivity with the excitation wavelength relative to R_O, the responsivity at 370 nm. The light intensity at different wavelengths are adjusted to be ~200 μ Wcm^{-2}. Inset: optical micrograph of the interdigitated electrodes fabricated on top of graphene. Scale bar: 100 μm. (b) Photocurrent as a function of source-drain bias (V_{DS}) for different light intensities. The applied V_G is 5 V.

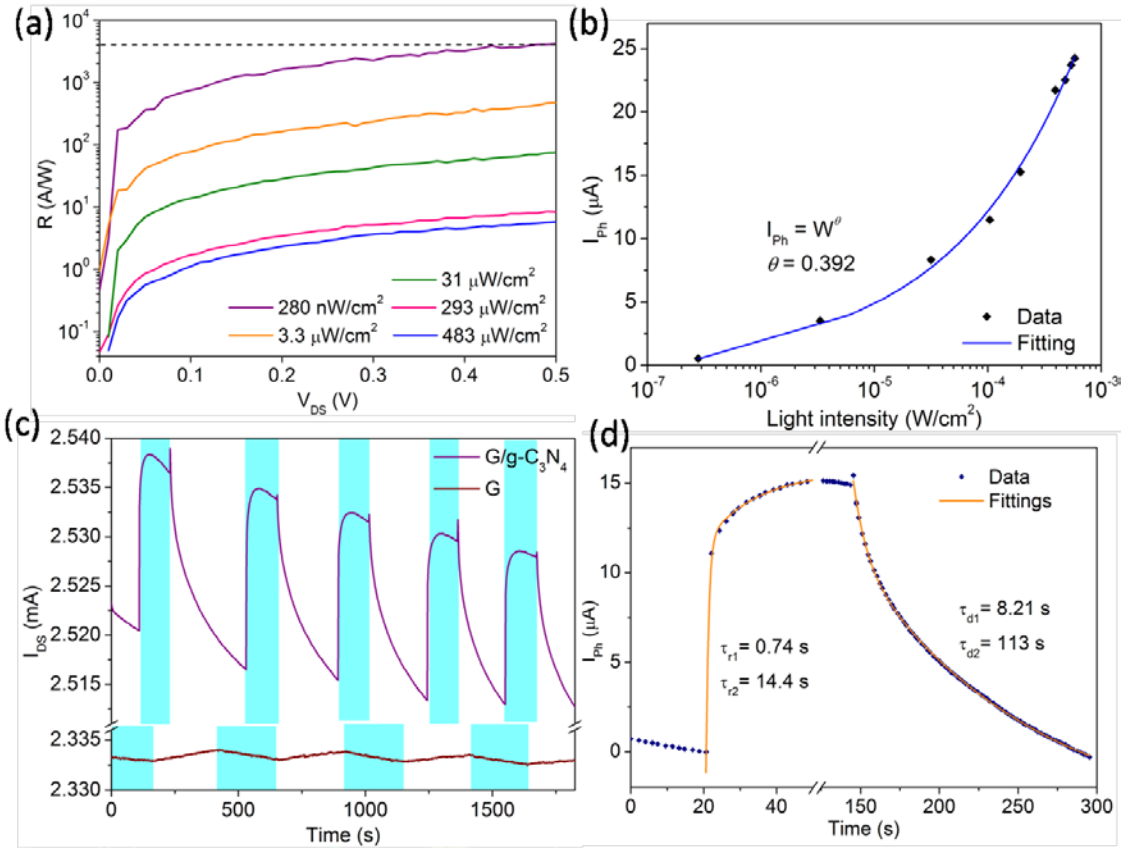

Figure 5. (a) Responsivity as a function of V_{DS}, showing the maximum responsivity of the device reaches 4×10^3 A/W. The applied V_G is 5 V. (b) Photocurrent as a function of light intensity fitted by the power law with the fitting parameters given in the graph. (c) Temporal response of the hybrid device that exhibit a positive photocurrent and a recoverable photoresponse, while the graphene-only control device exhibit a small negative photocurrent under the same biasing condition. The applied V_G is 8 V and V_{DS} is 0.5 V. The light intensity applied on hybrid device is 250 μWcm^{-2}, and that on graphene-only device is 585 μWcm^{-2}. (d) The response time analysis of the hybrid device.